THE JOURNAL OF PHYSICAL CHEMISTRY LETTERS
A JOURNAL OF THE AMERICAN CHEMICAL SOCIETY

pubs.acs.org/JPCL

Letter

Localization Mechanism of Interstitial Electronic States in Electride Mayenite

Dmitry Y. Novoselov,* Mary A. Mazannikova, Dmitry M. Korotin, Alexey O. Shorikov, Michael A. Korotin, Vladimir I. Anisimov, and Artem R. Oganov

Cite This: *J. Phys. Chem. Lett.* 2022, 13, 7155−7160

Read Online

ACCESS | Metrics & More | Article Recommendations

ABSTRACT: Electrides contain interstitial electrons with the states that are spatially separated from the crystal framework states and form a detached electronic subsystem. In mayenite $[Ca_{12}Al_{14}O_{32}]^{2+}(e^-)_2$ interstitial electrons form a unique charge network where localization and delocalization coexist, pointing to the importance of investigating the many-body nature of electride states. Using density functional theory and dynamical mean-field theory, we show a tendency toward electron localization and antiferromagnetic pairing, which leads to the formation of an experimentally observed peak under the Fermi level. The effect is associated with strong hybridization between interstitial electronic states, which removes the degeneracy and leads to the formation of a singlet state on a bonding molecular orbital as well as with the Coulomb interaction between interstitial electrons. Our work provides a fundamental understanding of the localization mechanism of interstitial electrons in mayenite and proposes a new approach for a proper description of the electronic subsystem of mayenite and other electrides.

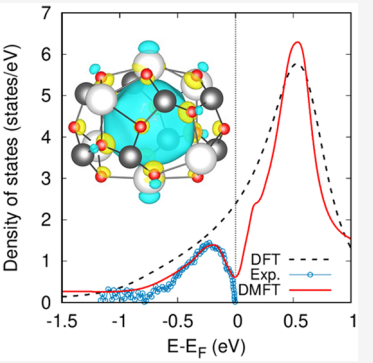

Mayenite (equivalent notations $Ca_{12}Al_{14}O_{33}$, $12CaO{\cdot}7Al_2O_3$, or C12A7) is an ionic framework of calcium aluminate with $I\bar{4}3d$ symmetry.[1−3] The structure of mayenite consists of 12 cages per unit cell. The cages have openings that look to each other and allow the extraction and loading of ions, which can then migrate through interconnected pores. Although the lattice framework has a positive charge, the cavities have statistically distributed counteranions (O^{2-}), which ensure the electroneutrality of the mineral as a whole.[2,4] The charged oxygen counteranions can be removed from the material as a neutral oxygen molecule and leave behind two excess electrons, which compensate the framework charge and convert mayenite into a zero-dimensional electride C12A7:e^-.[5] The crystal structure of C12A7:e^- can absorb up to 2.33×10^{21} cm^{-3} excess electrons.[6] The first fully reduced mayenite was obtained in 2003,[7] and it can be synthesized now directly from Al and commercially available precursors of CaO and Al_2O_3.[8] Because the mayenite framework is quite rigid, removing oxygen atoms from the cavities does not destroy it. Moreover, these cavities can embed,[9] for example, ions of gold, platinum, and chlorine as well as rare-earth elements, leading to a wide variety of technological applications, including promising field-emission properties[10,11] and prominent catalytic activity.[12−19] Mayenite, which is self-doped with electrons placed in positively charged cavities, can exhibit interesting physical properties such as low work function, a state of phonon glass and an electron crystal state,[20] a metal−insulator transition with a change in the concentration of interstitial electrons,[20] and superconductivity.[21−24] These properties of mayenite originate from the nesting of electride electrons in the cages weakly coupled to the lattice. These electrons form the energy states lying in the vicinity of the Fermi level.

The electronic structure of mayenite electride has been a subject of controversy in various theoretical studies. Early works[25−27] developed a model in which the electron density was mainly localized in cages, but mayenite turned out to be an insulator. It was shown[6] using different density functional theory (DFT) functionals that electride electrons are neither bound to specific atoms nor completely delocalized, but this was done separately for the fully localized insulating and uniformly delocalized metallic solutions. At the same time, another model was proposed[21,28] that employs a highly delocalized electron system that contradicts the notion that C12A7:e^- mayenite is an electride. Bader analysis[29] of the charge density distribution obtained by DFT did not find any non-nuclear attractors and the corresponding electride Bader basins in C12A7:e^-.[21] DFT calculations indicate that interstitial electrons are uniformly distributed between all cavities and do not have centers of localization, whereas neutron and synchrotron X-ray diffraction experiments[2] have shown that the electron density is

Received: June 28, 2022
Accepted: July 25, 2022
Published: July 29, 2022

https://doi.org/10.1021/acs.jpclett.2c02002
J. Phys. Chem. Lett. 2022, 13, 7155−7160

localized in the centers of cages. At the same time in another work[21] it was claimed that maximum entropy method (MEM)-Rietveld combined analyses of synchrotron powder X-ray diffraction patterns together with DFT calculations indicate that the electrons are delocalized over the cages. Furthermore, the results of the DFT[4,28,30,31] demonstrate a negative slope of the density of states (DOS) curve at the Fermi level, which indicates a negative sign of the Seebeck coefficient (charge carrier sign), while in the experiment[20,24] it is positive for the metallic phase of $[Ca_{12}Al_{14}O_{32}]^{2+}(e^-)_2$. Furthermore, using high-resolution photoemission spectroscopy, a small but well-defined peak at the Fermi level (E_F) was clearly observed,[31] while DFT[4,28,30,31] does not show any tendency to form such a peak. A probable reason lies in the fact that DFT tends to over-delocalize electron density due to the self-interaction error (SIE).[32] In this work, we reproduce a partially localized metallic state and elucidate the mechanism responsible for the localization of electride electrons. For this purpose, we studied the electronic structure associated with excess electrons describing them with Maximally-Localized Wannier Functions (MLWFs)[33] and considered them as a set of strongly hybridized molecular orbitals taking into account many-body correlation effects in the framework of Dynamical Mean-Field Theory (DMFT).[34,35]

The Wannier functions of excess anionic electrons in C12A7:e^- are centered at the 12*b* Wyckoff position of the $I\bar{4}3d$ group and are enclosed by the nearest axial calcium cations that form the first coordination sphere inside the cages. The latter being basic structural units of the mayenite framework with S_4 symmetry form periodic quasi-0D (0D = zero-dimensional) spaces (see inset in Figure 1). These states

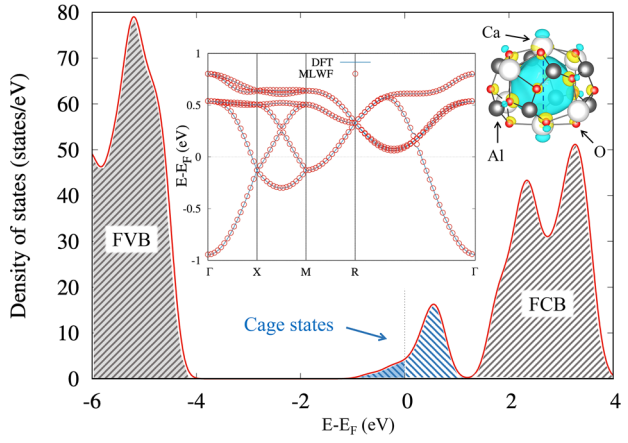

Figure 1. DFT density of states and band structure of $[Ca_{12}Al_{14}O_{32}]^{2+}(e^-)_2$ relative to the Fermi level (E_F). The contribution to the Bloch states by the MLWFs centered on the interstitial voids is shown by red circles. FVB and FCB are abbreviations of frame valence and frame conduction bands. (inset) Isosurface of a spatial distribution of a maximally localized Wannier function in a cage with its schematic view. The S_4 symmetry axis passes through the center of the cage, and the axial Ca atoms are denoted by the blue dashed line.

correspond to the energy bands crossing the Fermi level, well-separated from the frame valence and the frame conduction (FVBs and FCBs) bands and lying in the range from −1 to 1 eV relative to the Fermi level (Figure 1). To describe these electride electronic states, we constructed six MLWFs projected within the energy window spanned by six energy bands in the vicinity of E_F (Figure 1) and centered in the cavities (voids) (inset in Figure 1).[36−41] The obtained MLWFs represent the electride states and predominantly have an s-like orbital symmetry. These functions effectively contain contributions from the states of the frame atoms (yellow and blue areas of the isosurface in the inset of Figure 1). These contributions are due to the hybridization between the electride and atomic states and provide an interaction channel between the electrons localized in the neighboring cavities.

If electronic correlations are not taken into account, the electride states do not have a peak in the density of states below the Fermi level (Figure 1). We calculated the value of the Seebeck coefficient α solving the semiclassical Boltzmann transport equations[42] using the maximally localized Wannier function basis set and found that it has a negative sign $\alpha \approx -9$ μV/K at $T = 300$ K, while the experiment value of the Seebeck coefficient for the highest possible concentration of excess electrons is positive $\alpha = 10$ μV/K at $T = 300$ K.[20] The negative sign of the Seebeck coefficient indicates that the main type of charge carriers is electrons, while the experimental data[20] suggest that holes are the main carriers at the maximum possible concentration of electride electrons. All the Wannier functions obtained from the DFT calculation have the same occupancy, which is less than half-filling ($1/3e$). A change in the sign of the Seebeck coefficient from "−" to "+" is possible with more than half-filling of the corresponding states, and it could be realized in the case of a nonuniform redistribution of electrons between different electride states in favor of one of them.

The obtained MLWFs were used as a basis to construct the non-interacting Hamiltonian. All the diagonal elements of this Hamiltonian have the same value, and if off-diagonal elements were absent in the Hamiltonian, then these states would be degenerate. However, hybridization between the electride orbitals of neighboring cavities, which lifts the degeneracy of electride states, leads to the presence of such off-diagonal elements corresponding to electron hoppings between cavities. These elements reflect essential information about an intrinsic symmetry of the electride electronic subsystem and intercage electronic hoppings, which can be described as a charge network. These interactions can be taken into account considering the electride electron subsystem as a cluster[25] or a molecule.[43,44]

For this purpose, we employed the combination of density functional theory and dynamical mean field theory, the so-called DFT+DMFT method.[45−47] The continuous-time quantum Monte Carlo (CT-QMC)[48] solver, which treats the diagonal elements of Green's function only, was used to solve an effective DMFT quantum impurity problem.[49] In order to map a cluster model to a local problem at the first step we diagonalize the Hamiltonian. This transformation, which is mathematically rigorous, could be considered as a transition into the basis of the molecular orbitals[43,44] that form the charge network of electride. In this basis the off-diagonal elements of Green's function are negligible, and the lack of degeneracy of electride states and all interactions between them are contained in diagonal elements of Green's function. In this case, using the diagonal solver does not lead to errors in the description of electride states. We set interorbital parameter U' equal to intraorbital parameter U in all sets of calculations. Calculations were performed for several values of the Coulomb parameter U, which acts as an effective interaction parameter between electrons localized on molecular orbitals. Accounting for correlation effects leads to the localization and spin pairing of interstitial electrons on one molecular orbital, while the rest of the interstitial electrons

https://doi.org/10.1021/acs.jpclett.2c02002
J. Phys. Chem. Lett. 2022, 13, 7155−7160

remain only partially localized, providing a nonzero density of states at the Fermi level and metallic character. This scenario is reminiscent of the orbital-selective Mott transition model proposed for $(Ca,Sr)_2RuO_4$.[50] The degree of localization and emergence of electron singlet depends on the value of the interaction parameter U. Such behavior indicates a tendency toward the formation of diamagnetic electron pairs with antiparallel spins or a singlet polaron, which is consistent with the experimental observations.[5]

To analyze changes in the density of electride electronic states that arise as a result of accounting for many-body effects, the spectral functions were evaluated using an analytical continuation of the self-energy dependences on the real frequencies (Figure 2). It can be seen from Figure 2 that, unlike DFT, a well-

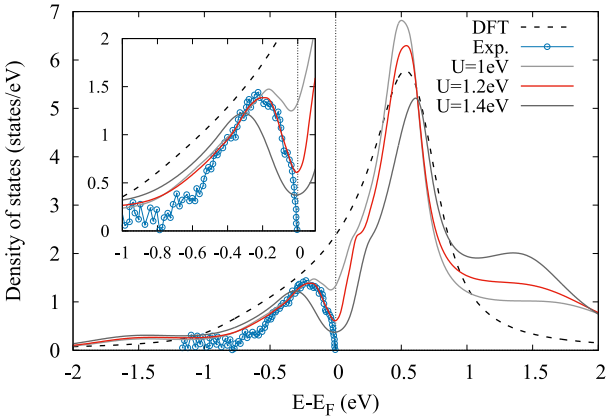

Figure 2. Total density of electride states obtained by DFT (black dashed curve) and by DMFT with different U values (solid curves) as well as the experimental data[31] marked with blue circles. (inset) An enlarged region below the Fermi level.

pronounced peak directly below the Fermi level is formed in DMFT in the energy range of the cage valence band. The position of this peak depends on the value of the Coulomb parameter U. The best agreement of the peak position with the results of the photoemission spectroscopy experiments[31] is achieved for $U = 1.2$ eV. The valley-like shape of the DOS at E_F also agrees with the Seebeck coefficient measurements.[20,24] The formation of the peak below the Fermi level in DMFT indicates that localization of electride electrons was caused by correlation effects and can emerge even without structural distortions, that is, cage compression around localized electrons.

In DMFT, 1.61 out of 2 anionic electrons are localized at the bonding molecular orbital, clearly indicating the presence of antiferromagnetic electron pairing. It is worth noting that the energy spectrum tends to form a pseudogap between the bonding and antibonding states, while the remaining four orbitals form a common peak at 0.5 eV above the Fermi level and are nonbonding states.

The DMFT k-resolved spectral function for $U = 1.2$ eV, which might be compared directly to angle-resolved photoemission spectroscopy (ARPES), is shown in Figure 3. It demonstrates strong thermal smearing, which is responsible for the pseudogap in the DMFT DOS in contrast to the DFT bands (shown with circles). One can see an almost separated flat band just below the Fermi level, which corresponds to the broad band in the DMFT spectral function (see Figure 2), which spreads from −2 eV to the Fermi level with a pronounced peak.

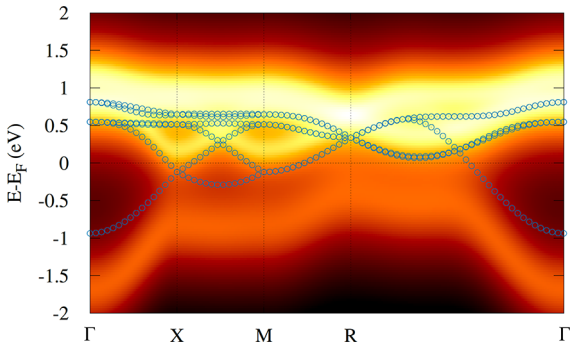

Figure 3. k-Resolved total spectral function $A(k, \omega)$ of $[Ca_{12}Al_{14}O_{32}]^{2+}(e^-)_2$ along the Γ-X-M-R-Γ direction obtained by DFT+DMFT for $U = 1.2$ eV; the DFT band structure is shown with blue circles.

DMFT calculations of mayenite electride also show that taking into account the many-body correlation effects leads to an energy gain equal to −0.5935 (±0.0003) eV/cell due to the increased localization of the electronic states, indicating the favorability of this process.

The formation of localized electron diamagnetic pairs will lead to inhomogeneity of the electron density distribution within the charge network. This will cause corresponding structural distortions accompanied predominantly by compression of some cages along the S_4 symmetry axis[6,21,25] passing through the center of the cage and two axial calcium atoms due to electrostatic attraction between them and interstitial electrons. Inhomogeneous lattice distortions facilitate the localization of out-of-framework electrons at the distorted lattice cages.[6] Such an observation corresponds to a polaron formation that agrees with the polaron-type electronic conductivity.[6,51,52] Thus, the next stage of research could be complete charge-self-consistent DFT+DMFT calculations, which would give a more accurate crystal structure and related electronic properties.

In the case of less than half-filling, DFT does not allow one to obtain a localized singlet electron state due to the absence of a pairing potential. To analyze and illustrate the mechanism of an antiferromagnetic electron pairing observed in the electride subsystem of mayenite, we present a minimal ad hoc three-band model with semicircular density of states $DOS_i(\varepsilon)=2/\pi D_i \times\sqrt{1-(\varepsilon/D_i)^2}$, where $2D_i$ is the bandwidth W. We set $W = 2$ eV; interband Coulomb repulsion U' was varied from 0 to 1.8 eV, and intraband U was set to 1.2 eV. These values were chosen to reproduce the DOS from DFT and the behavior of a real electride when using DMFT. If we treat the electride subsystem as a charge network, then nonzero off-diagonal elements of the Hamiltonian will lead to the appearance of bonding, antibonding, and nonbonding molecular orbitals. To reproduce this picture for the case of nondegenerate bands we introduce the additional splitting of $\Delta = \pm 0.9$ eV. The filling was set to two electrons in all cases. This model was solved by DMFT for $\beta = 10$ eV^{-1} using CT-QMC solver. This solver allows one to calculate not only magnetic and spectral properties but also the probabilities (statistical weights) of different electronic configurations. The results of the calculations are presented in Figure 4.

This simple model can reproduce the formation of paired states with a small number of adjustable parameters. In the case of fully degenerate bands with two electrons and only intraband U taken into account we obtain a metallic state with negligible

https://doi.org/10.1021/acs.jpclett.2c02002
J. Phys. Chem. Lett. 2022, 13, 7155−7160

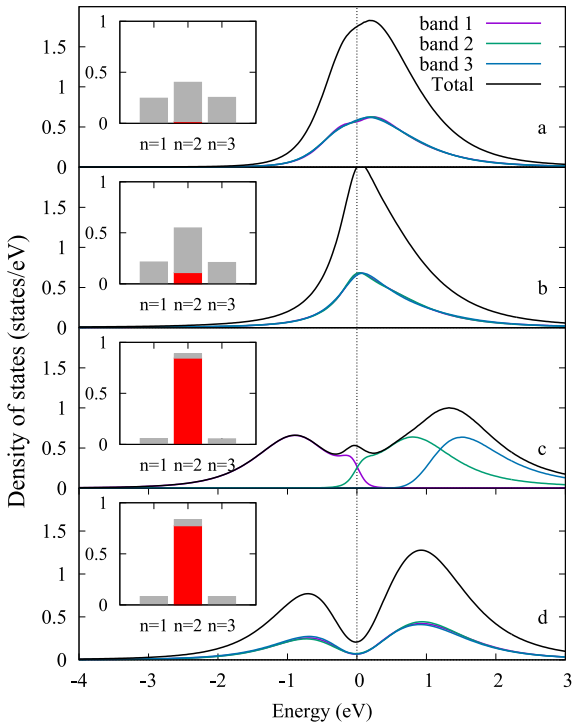

Figure 4. DOS of the model obtained by DMFT with $U = 1.2$ eV and (a) $U' = 0$ eV, $\Delta = 0$ eV, (b) $U' = 1.2$ eV, $\Delta = 0$ eV, (c) $U' = 1.2$ eV, $\Delta = \pm 0.9$ eV, and (d) $U' = 1.8$ eV, $\Delta = 0$ eV. (insets) Weights of configurations with different numbers of electrons. The red shading corresponds to the weight of the paired state.

weight of the state with paired electrons (see Figure 4a). This solution matches the expectation for the model with $U/W < 1$. It is worth noting that the weights of configurations with a total number of electrons of 1 and 2 are significant, which indicates that electrons are itinerant.

An increase in the interband repulsion parameter U' up to 1.2 eV (Figure 4b) does not qualitatively change the result. The system remains metallic, but the weight of the paired electrons becomes 0.11, which can be interpreted as the threshold for the formation of a singlet state. The mean-squared magnetic moment $\langle m_z^2 \rangle$ for these two cases is 1.76 and 1.50 $\mu_B{}^2$, respectively, which also indicates the absence of a paired state. A further increase of U' to 1.8 eV (Figure 4d) drastically changes the result. A singlet paired state with a weight of 0.78 appears, and the value of $\langle m_z^2 \rangle$ drops to 0.29 $\mu_B{}^2$. Also, a pseudogap at the Fermi level is formed. In the case of a nondegenerate model, the pairing of electrons with the formation of a pseudogap state can occur for lower $U' = 1.2$ eV (Figure 4c). The small value of the mean square of the magnetic moment $\langle m_z^2 \rangle = 0.2\ \mu_B{}^2$ also shows that two electrons form a singlet state. This can be explained by the fact that the scaling of the critical U parameter in the Hubbard model is necessary for the metal−insulator transition as follows: $U_c = \sqrt{N} U_c^{N=1}$, where N is degeneracy, and $U_c^{N=1}$ is the critical value for the nondegenerate case.[53]

Thus, the mechanism of localization of a diamagnetic pair in mayenite is based on strong hybridization between electride states, which removes the degeneracy and facilitates the formation of a singlet state in the bonding molecular orbital as well as the presence of the Coulomb interaction between electride electrons both inside one cage and between adjacent ones.

The results obtained in this work clearly demonstrate the tendency toward the formation of electride diamagnetic pairs in C12A7:e^- with electron anions coupled antiferromagnetically with each other ($S = 0$),[5] which, in particular, may be in favor of the bipolaronic mechanism[54] of superconductivity in mayenite. The localization of electride states in mayenite, together with the data obtained earlier[55−59] for other electrides, allows us to suggest the importance of taking into account many-particle correlation effects when considering the electride subsystem.

In summary, using the DFT+DMFT approach, we showed a clear trend toward localization and antiferromagnetic electron pairing in the C12A7:e^- mayenite electride. This effect is based on both strong hybridization between interstitial electronic states, which lifts the degeneracy of the electronic subsystem and leads to the formation of a singlet state on the bonding molecular orbital, and the presence of the Coulomb interaction between electrons on the electride state and between neighboring cages. Some of the electrons maintain a partially delocalized character, providing a nonzero density of states at the Fermi level. This leads to the formation of the experimentally observed peak[31] in the cage valence band just below the Fermi level together with the metallicity. Thus, we found that many-body correlation effects in the subspace of the electride charge network are a crucial part of the physics that defines important properties of electride mayenite.

COMPUTATIONAL METHODS

As the first step, a non-interacting DFT band structure $\varepsilon(\vec{k})$ was obtained using the VASP package[60] with the exchange-correlation energy described by the generalized gradient approximation (GGA) and the Perdew−Burke−Ernzerhof (PBE) functional.[61] The initial structural data for $[Ca_{12}Al_{14}O_{32}]^{2+}(e^-)_2$, which has equal cages, were taken from ref 2. Integration in the reciprocal space was performed on a regular $4 \times 4 \times 4$ k-point mesh in the irreducible part of the Brillouin zone. The MLWF basis was obtained using the Wannier90 package,[37] which was also used to extract the non-interacting GGA Hamiltonian H_{GGA} in the real space. The obtained Hamiltonian was transformed into the reciprocal space on a regular $12 \times 12 \times 12$ k-point mesh and then diagonalized, which makes off-diagonal elements of Green's function negligible and allows one to use the diagonal solver. The DFT+DMFT approach[45,46] was used to take into account Coulomb correlations and many-body effects for the constructed Hamiltonian. DFT+DMFT calculations were performed for the inverse temperature $\beta = 1/k_BT = 20$ eV^{-1}, where k_B is the Boltzmann constant and T is the absolute temperature. The effective DMFT quantum impurity problem[49] was solved using the continuous-time quantum Monte Carlo method with the hybridization expansion algorithm[48] as realized in the package AMULET.[47] The analytical continuation of a self-energy dependence from Matsubara to the real frequencies was evaluated using the Padé approximation method.[62] The electronic transport properties were evaluated in a semiclassical transport framework using an MLWF basis for the band structure interpolation and the calculation of band velocities within BoltzWann.[42]

AUTHOR INFORMATION

Corresponding Author

Dmitry Y. Novoselov − *M. N. Mikheev Institute of Metal Physics, Ural Branch of Russian Academy of Sciences, Yekaterinburg 620108, Russia; Department of theoretical*

https://doi.org/10.1021/acs.jpclett.2c02002
J. Phys. Chem. Lett. 2022, 13, 7155−7160

physics and applied mathematics, Ural Federal University, Yekaterinburg 620002, Russia; Skolkovo Institute of Science and Technology, Moscow 143026, Russia; orcid.org/0000-0003-1668-3734; Email: novoselov@imp.uran.ru

Authors

Mary A. Mazannikova − *M. N. Mikheev Institute of Metal Physics, Ural Branch of Russian Academy of Sciences, Yekaterinburg 620108, Russia; Department of theoretical physics and applied mathematics, Ural Federal University, Yekaterinburg 620002, Russia;* orcid.org/0000-0003-1418-4018

Dmitry M. Korotin − *M. N. Mikheev Institute of Metal Physics, Ural Branch of Russian Academy of Sciences, Yekaterinburg 620108, Russia; Skolkovo Institute of Science and Technology, Moscow 143026, Russia;* orcid.org/0000-0002-4070-2045

Alexey O. Shorikov − *M. N. Mikheev Institute of Metal Physics, Ural Branch of Russian Academy of Sciences, Yekaterinburg 620108, Russia; Department of theoretical physics and applied mathematics, Ural Federal University, Yekaterinburg 620002, Russia; Skolkovo Institute of Science and Technology, Moscow 143026, Russia*

Michael A. Korotin − *M. N. Mikheev Institute of Metal Physics, Ural Branch of Russian Academy of Sciences, Yekaterinburg 620108, Russia;* orcid.org/0000-0002-9603-8374

Vladimir I. Anisimov − *M. N. Mikheev Institute of Metal Physics, Ural Branch of Russian Academy of Sciences, Yekaterinburg 620108, Russia; Department of theoretical physics and applied mathematics, Ural Federal University, Yekaterinburg 620002, Russia; Skolkovo Institute of Science and Technology, Moscow 143026, Russia*

Artem R. Oganov − *Skolkovo Institute of Science and Technology, Moscow 143026, Russia;* orcid.org/0000-0001-7082-9728

Complete contact information is available at: https://pubs.acs.org/10.1021/acs.jpclett.2c02002

Notes

The authors declare no competing financial interest.

■ ACKNOWLEDGMENTS

The authors thank S. V. Streltsov for useful discussion. The DFT and MLWF parts of the study were supported by the Ministry of Science and Higher Education of the Russian Federation (No. 122021000039-4, theme "Electron"). The DMFT results were obtained within the state assignment of the Russian Science Foundation (Project No. 19-72-30043).

■ REFERENCES

(1) Dye, J. L. Chemistry: Electrons as Anions. *Science* **2003**, *301*, 607−608.

(2) Palacios, L.; De La Torre, Á. G.; Bruque, S.; García-Muñoz, J. L.; García-Granda, S.; Sheptyakov, D.; Aranda, M. A. Crystal structures and in-situ formation study of mayenite electrides. *Inorg. Chem.* **2007**, *46*, 4167−4176.

(3) Boysen, H.; Lerch, M.; Stys, A.; Senyshyn, A. Structure and oxygen mobility in mayenite ($Ca_{12}Al_{14}O_{33}$): A high-temperature neutron powder diffraction study. *Acta Crystallographica Section B: Structural Science* **2007**, *63*, 675−682.

(4) Yu, Z.; Okoronkwo, M. U.; Sant, G.; Misture, S. T.; Wang, B. Understanding Oxygen Nonstoichiometry in Mayenite: From Electride to Oxygen Radical Clathrate. *J. Phys. Chem. C* **2019**, *123*, 11982−11992.

(5) Matsuishi, S.; Toda, Y.; Miyakawa, M.; Hayashi, K.; Kamiya, T.; Hirano, M.; Tanaka, I.; Hosono, H. High-Density Electron Anions in a Nanoporous Single Crystal: $[Ca_{24}Al_{28}O_{64}]^{4+}(4e^-)$. *Science* **2003**, *301*, 626−629.

(6) Sushko, P. V.; Shluger, A. L.; Hirano, M.; Hosono, H. From insulator to electride: A theoretical model of nanoporous oxide $12CaO·7Al_2O_3$. *J. Am. Chem. Soc.* **2007**, *129*, 942−951.

(7) Matsuishi, S.; Toda, Y.; Miyakawa, M.; Hayashi, K.; Kamiya, T.; Hirano, M.; Tanaka, I.; Hosono, H. High-Density Electron Anions in a Nanoporous Single Crystal: $[Ca_{24}Al_{28}O_{64}]^{4+}(4e^-)$. *Science* **2003**, *301*, 626−629.

(8) Li, F.; Zhang, X.; Liu, H. Insights into the direct formation of $[Ca_{24}Al_{28}O_{64}]^{4+}(4e)$ and its electrical characterization. *J. Am. Ceram. Soc.* **2020**, *103*, 35−42.

(9) Nakao, T.; Ogasawara, K.; Kitano, M.; Matsuishi, S.; Sushko, P. V.; Hosono, H. Ship-in-a-Bottle Synthesis of High Concentration of N_2 Molecules in a Cage-Structured Electride. *J. Phys. Chem. Lett.* **2021**, *12*, 1295−1299.

(10) Toda, Y.; Matsuishi, S.; Hayashi, K.; Ueda, K.; Kamiya, T.; Hirano, M.; Hosono, H. Field Emission of Electron Anions Clathrated in Subnanometer-Sized Cages in $[Ca_{24}Al_{28}O_{64}]^{4+}(4e^-)$. *Adv. Mater.* **2004**, *16*, 685−689.

(11) Toda, Y.; Kim, S. W.; Hayashi, K.; Hirano, M.; Kamiya, T.; Hosono, H.; Haraguchi, T.; Yasuda, H. Intense thermal field electron emission from room-temperature stable electride. *Appl. Phys. Lett.* **2005**, *87*, 254103.

(12) Wang, Z.; Pan, Y.; Dong, T.; Zhu, X.; Kan, T.; Yuan, L.; Torimoto, Y.; Sadakata, M.; Li, Q. Production of hydrogen from catalytic steam reforming of bio-oil using C12A7-O−based catalysts. *Applied Catalysis A: General* **2007**, *320*, 24−34.

(13) Kitano, M.; Inoue, Y.; Yamazaki, Y.; Hayashi, F.; Kanbara, S.; Matsuishi, S.; Yokoyama, T.; Kim, S. W.; Hara, M.; Hosono, H. Ammonia synthesis using a stable electride as an electron donor and reversible hydrogen store. *Nat. Chem.* **2012**, *4*, 934−940.

(14) Hara, M.; Kitano, M.; Hosono, H. Ru-Loaded C12A7:e^- Electride as a Catalyst for Ammonia Synthesis. *ACS Catal.* **2017**, *7*, 2313−2324.

(15) Khan, K.; Tareen, A. K.; Aslam, M.; Thebo, K. H.; Khan, U.; Wang, R.; Shams, S. S.; Han, Z.; Ouyang, Z. A comprehensive review on synthesis of pristine and doped inorganic room temperature stable mayenite electride, $[Ca_{24}Al_{28}O_{64}]^{4+}(4e)$ and its applications as a catalyst. *Prog. Solid State Chem.* **2019**, *54*, 1−19.

(16) Inoue, Y.; Kitano, M.; Tokunari, M.; Taniguchi, T.; Ooya, K.; Abe, H.; Niwa, Y.; Sasase, M.; Hara, M.; Hosono, H. Direct Activation of Cobalt Catalyst by $12CaO·7Al_2O_3$ Electride for Ammonia Synthesis. *ACS Catal.* **2019**, *9*, 1670−1679.

(17) Marakatti, V. S.; Gaigneaux, E. M. Recent Advances in Heterogeneous Catalysis for Ammonia Synthesis. *ChemCatChem.* **2020**, *12*, 5838−5857.

(18) Hosono, H.; Kitano, M. Advances in Materials and Applications of Inorganic Electrides. *Chem. Rev.* **2021**, *121*, 3121−3185.

(19) Gong, Y.; Li, H.; Wu, J.; Song, X.; Yang, X.; Bao, X.; Han, X.; Kitano, M.; Wang, J.; Hosono, H. Unique Catalytic Mechanism for Ru-Loaded Ternary Intermetallic Electrides for Ammonia Synthesis. *J. Am. Chem. Soc.* **2022**, *144*, 8683−8692.

(20) Kim, S. W.; Tarumi, R.; Iwasaki, H.; Ohta, H.; Hirano, M.; Hosono, H. Thermal conductivity and Seebeck coefficient of mayenite $12CaO·7Al_2O_3$ with a cage structure. *Phys. Rev. B* **2009**, *80*, 075201.

(21) Kim, S. W.; Matsuishi, S.; Nomura, T.; Kubota, Y.; Takata, M.; Hayashi, K.; Kamiya, T.; Hirano, M.; Hosono, H. Metallic state in a lime-alumina compound with nanoporous structure. *Nano Lett.* **2007**, *7*, 1138−1143.

(22) Kim, S. W.; Hosono, H. Synthesis and properties of $12CaO · 7Al_2O_3$ electride: Review of single crystal and thin film growth. *Philos. Mag.* **2012**, *92*, 2596−2628.

(23) Miyakawa, M.; Kim, S. W.; Hirano, M.; Kohama, Y.; Kawaji, H.; Atake, T.; Ikegami, H.; Kono, K.; Hosono, H. Superconductivity in an Inorganic Electride $12CaO·7Al_2O_3:e^-$. *J. Am. Chem. Soc.* **2007**, *129*, 7270−7271.

(24) Hosono, H.; Kim, S.-W.; Matsuishi, S.; Tanaka, S.; Miyake, A.; Kagayama, T.; Shimizu, K. Superconductivity in room-temperature stable electride and high-pressure phases of alkali metals. *Philosophical Transactions of the Royal Society A: Mathematical, Physical and Engineering Sciences* **2015**, *373*, 20140450.
(25) Sushko, P. V.; Shluger, A. L.; Hayashi, K.; Hirano, M.; Hosono, H. Electron localization and a confined electron gas in nanoporous inorganic electrides. *Phys. Rev. Lett.* **2003**, *91*, 10−13.
(26) Kamiya, T.; Hosono, H. Built-in Quantum Dots in Nano-Porous Crystal $12CaO{\cdot}7Al_2O_3$: Simplified Views for Electronic Structure and Carrier Transport. *Jpn. J. Appl. Phys.* **2005**, *44*, 774−782.
(27) Sushko, P. V.; Shluger, A. L.; Hirano, M.; Hosono, H. From Insulator to Electride: A Theoretical Model of Nanoporous Oxide $12CaO{\cdot}7Al_2O_3$. *J. Am. Chem. Soc.* **2007**, *129*, 942−951.
(28) Medvedeva, J. E.; Freeman, A. J. Hopping versus bulk conductivity in transparent oxides: $12CaO7Al_2O_3$. *Appl. Phys. Lett.* **2004**, *85*, 955−957.
(29) Bader, R. F. W. A quantum theory of molecular structure and its applications. *Chem. Rev.* **1991**, *91*, 893−928.
(30) Kamiya, T. Natural nanostructures in ionic semiconductors. *Microelectron. Eng.* **2004**, *73*−*74*, 620−626.
(31) Souma, S.; Arakane, T.; Sato, T.; Takahashi, T.; Wng Kim, S.; Matsuishi, S.; Hosono, H. Direct Evidence for Cage Conduction Band in Superconducting Cement $12CaO{\cdot}7Al_2O_3$ by Low-Energy High-Resolution Photoemission Spectroscopy. *J. Phys. Soc. Jpn.* **2010**, *79*, 103704.
(32) Bao, J. L.; Gagliardi, L.; Truhlar, D. G. Self-Interaction Error in Density Functional Theory: An Appraisal. *J. Phys. Chem. Lett.* **2018**, *9*, 2353−2358.
(33) Marzari, N.; Mostofi, A. A.; Yates, J. R.; Souza, I.; Vanderbilt, D. Maximally localized Wannier functions: Theory and applications. *Rev. Mod. Phys.* **2012**, *84*, 1419−1475.
(34) Kotliar, G.; Vollhardt, D. Strongly Correlated Materials: Insights From Dynamical Mean-Field Theory. *Phys. Today* **2004**, *57*, 53−59.
(35) Georges, A.; Kotliar, G.; Krauth, W.; Rozenberg, M. J. Dynamical mean-field theory of strongly correlated fermion systems and the limit of infinite dimensions. *Rev. Mod. Phys.* **1996**, *68*, 13−125.
(36) Marzari, N.; Vanderbilt, D. Maximally localized generalized Wannier functions for composite energy bands. *Phys. Rev. B* **1997**, *56*, 12847−12865.
(37) Mostofi, A. A.; Yates, J. R.; Pizzi, G.; Lee, Y.-S.; Souza, I.; Vanderbilt, D.; Marzari, N. An updated version of wannier90: A tool for obtaining maximally-localised Wannier functions. *Comput. Phys. Commun.* **2014**, *185*, 2309−2310.
(38) Novoselov, D. Y.; Korotin, D. M.; Shorikov, A. O.; Anisimov, V. I. Charge and spin degrees of freedom in strongly correlated systems: Mott states opposite Hundas metals. *J. Phys.: Condens. Matter* **2020**, *32*, 235601.
(39) Novoselov, D.; Korotin, D. M.; Anisimov, V. I. Spin state transition in the active center of the hemoglobin molecule: DFT + DMFT study. *JETP Letters* **2016**, *103*, 658−662.
(40) Novoselov, D.; Korotin, D. M.; Anisimov, V. I. Hellmann-Feynman forces within the DFT+U in Wannier functions basis. *J. Phys.: Condens. Matter* **2015**, *27*, 325602.
(41) Korotin, D. M.; Novoselov, D.; Anisimov, V. I. Correlation effects and phonon modes softening with doping in $Ba_{1-x}K_xBiO_3$. *J. Phys.: Condens. Matter* **2014**, *26*, 195602.
(42) Pizzi, G.; Volja, D.; Kozinsky, B.; Fornari, M.; Marzari, N. BoltzWann: A code for the evaluation of thermoelectric and electronic transport properties with a maximally-localized Wannier functions basis. *Comput. Phys. Commun.* **2014**, *185*, 422−429.
(43) Florens, S. Nanoscale Dynamical Mean-Field Theory for Molecules and Mesoscopic Devices in the Strong-Correlation Regime. *Phys. Rev. Lett.* **2007**, *99*, 046402.
(44) Turkowski, V.; Kabir, A.; Nayyar, N.; Rahman, T. S. Dynamical mean-field theory for molecules and nanostructures. *J. Chem. Phys.* **2012**, *136*, 114108.
(45) Anisimov, V. I.; Poteryaev, A. I.; Korotin, M. A.; Anokhin, A. O.; Kotliar, G. First-principles calculations of the electronic structure and spectra of strongly correlated systems: dynamical mean-field theory. *J. Phys.: Condens. Matter* **1997**, *9*, 7359−7367.
(46) Held, K.; Nekrasov, I. A.; Keller, G.; Eyert, V.; Blümer, N.; McMahan, A. K.; Scalettar, R. T.; Pruschke, T.; Anisimov, V. I.; Vollhardt, D. Realistic investigations of correlated electron systems with LDA+DMFT. *physica status solidi (b)* **2006**, *243*, 2599−2631.
(47) *Amulet*. http://www.amulet-code.org accessed on June 28, 2022.
(48) Gull, E.; Millis, A. J.; Lichtenstein, A. I.; Rubtsov, A. N.; Troyer, M.; Werner, P. Continuous-time Monte Carlo methods for quantum impurity models. *Rev. Mod. Phys.* **2011**, *83*, 349−404.
(49) Werner, P.; Millis, A. J. Hybridization expansion impurity solver: General formulation and application to Kondo lattice and two-orbital models. *Phys. Rev. B* **2006**, *74*, 155107.
(50) Anisimov, V.; Nekrasov, I.; Kondakov, D.; Rice, T.; Sigrist, M. Orbital-selective Mott-insulator transition in $Ca_{2-x}Sr_xRuO_4$. *European Physical Journal B* **2002**, *25*, 191−201.
(51) Anderson, M. S. Electride mediated surface enhanced Raman scattering. *Appl. Phys. Lett.* **2013**, *103*, 131103.
(52) Lobo, R. P.; Bontemps, N.; Bertoni, M. I.; Mason, T. O.; Poeppelmeier, K. R.; Freeman, A. J.; Park, M. S.; Medvedeva, J. E. Optical conductivity of mayenite: From insulator to metal. *J. Phys. Chem. C* **2015**, *119*, 8849−8856.
(53) Han, J. E.; Jarrell, M.; Cox, D. L. Multiorbital Hubbard model in infinite dimensions: Quantum Monte Carlo calculation. *Phys. Rev. B* **1998**, *58*, R4199−R4202.
(54) Edwards, P. P.; Rao, C. N. R.; Kumar, N.; Alexandrov, A. S. The Possibility of a Liquid Superconductor. *ChemPhysChem* **2006**, *7*, 2015−2021.
(55) Novoselov, D. Y.; Korotin, D. M.; Shorikov, A. O.; Oganov, A. R.; Anisimov, V. I. Interplay Between Coulomb Interaction and Hybridization in Ca and Anomalous Pressure Dependence of Resistivity. *JETP Letters* **2019**, *109*, 387−391.
(56) Novoselov, D. Y.; Korotin, D. M.; Shorikov, A. O.; Oganov, A. R.; Anisimov, V. I. Weak Coulomb correlations stabilize the electride high-pressure phase of elemental calcium. *J. Phys.: Condens. Matter* **2020**, *32*, 445501.
(57) Novoselov, D. Y.; Korotin, D. M.; Shorikov, A. O.; Anisimov, V. I.; Oganov, A. R. Interacting Electrons in Two-Dimensional Electride Ca_2N. *J. Phys. Chem. C* **2021**, *125*, 15724−15729.
(58) Novoselov, D. Y.; Anisimov, V. I.; Oganov, A. R. Strong electronic correlations in interstitial magnetic centers of zero-dimensional electride β-Yb_5Sb_3. *Phys. Rev. B* **2021**, *103*, 235126.
(59) Kanno, S.; Tada, T.; Utsumi, T.; Nakamura, K.; Hosono, H. Electronic Correlation Strength of Inorganic Electrides from First Principles. *J. Phys. Chem. Lett.* **2021**, *12*, 12020−12025.
(60) Kresse, G.; Furthmüller, J. Efficient iterative schemes for ab initio total-energy calculations using a plane-wave basis set. *Phys. Rev. B* **1996**, *54*, 11169−11186.
(61) Perdew, J. P.; Burke, K.; Ernzerhof, M. Generalized Gradient Approximation Made Simple. *Phys. Rev. Lett.* **1996**, *77*, 3865−3868.
(62) Vidberg, H. J.; Serene, J. W. Solving the Eliashberg equations by means of N-point Pade approximants. *Journal of Low Temperature Physics* **1977**, *29*, 179−192.

https://doi.org/10.1021/acs.jpclett.2c02002
J. Phys. Chem. Lett. 2022, 13, 7155−7160